International Journal of Civil Engineering
https://doi.org/10.1007/s40999-023-00880-y

RESEARCH PAPER

Experimental and Numerical Analyses of Two Instrumented Large Diameter Drilled Shafts Under Bidirectional Static Loading Test

Yuri Barbosa[1] · Paulo José Rocha Albuquerque[1] · Nilton Andrade Chaves[2]

Received: 19 September 2022 / Revised: 18 April 2023 / Accepted: 28 July 2023

Abstract
This article presents the results of bidirectional static loading test carried out on two drilled shafts of 1.6 m in diameter, which were instrumented along the depth for analysis of the mechanical behavior (final lengths of 48.4 m and 48.8 m). The tests were carried out up to the load of 18,400 and 13,200 kN, respectively. Due to the longer delay between drilling and concreting in the first case, results of the instrumentations indicated that no tip resistance was mobilized, mobilizing its side resistance of the upper segment up to 90 kPa, while in the second case, this value was around 60 kPa and 150 kPa for its tip resistance. The stabilizing polymer used for drilling affected the shaft resistance of both piles. In addition, in the last case studied, the total loss of contact at the pile–soil interface between the load application point and the instrumented level just above allowed the evaluation of the possible existence of residual loads along the shaft. Load-transfer curves were approximated in hyperbolic functions, and a load-transfer model was implemented for data validation and equivalent load–displacement curve estimating, showing good agreement between load tests and simulations. This model indicated that the upper segment load–displacement curve of the second case was displaced by 1150 kN due to the possible residual load, and the ultimate bearing capacity for both piles under conventional loading was 23,000 and 26,600 kN, respectively.

Keywords Bidirectional test · Drilled shaft · Instrumentation · Load-transfer model

1 Introduction

The use of large diameter drilled shafts has grown in Brazil due to their characteristic resistance to large loads at small displacement rates in the superstructure. Usually, this type of pile is used for large-scale works, such as large buildings and bridges [1–5]—constructions that, in most cases, are made in sedimentary soils of coastal regions. Due to the presence of the water table at low depths in these regions and the extensive lengths of these types of piles, the use of stabilizing fluid is necessary during the excavation process which, in turn, can compromise the development of skin friction along their shafts [4–7]. In addition, the perforation with layers of sand promotes the deposit of debris and loose material inside the borehole, which settles at the pile tip and impairs the mobilization of its resistance portion. This fact makes the load capacity of the tip of large diameter drilled shafts difficult to estimate and, despite its high resistance potential especially when socketed in rock profiles, a significant part of this resistance is disregarded in designs of this type of pile [8]. For these reasons, large diameter drilled shafts must be tested before continuing any work to verify the estimated design load capacity. However, due to its high load capacity, conventional static load tests become unfeasible as they require a robust reaction system, thus increasing the costs and safety risks of the test, which favors the use of bidirectional tests.

The bidirectional static load test (BDSLT) began in the 1980s in Brazil with the work of Silva [9] and, at the same

✉ Paulo José Rocha Albuquerque
pjra@unicamp.br

Yuri Barbosa
y209352@g.unicamp.br

Nilton Andrade Chaves
nilton.chaves@arcos.eng.br

[1] School of Civil Engineering, Architecture and Urban Design, Department of Infrastructure and Environment, University of Campinas, 224, Saturnino de Brito St., Campinas, São Paulo 13083-889, Brazil

[2] Arcos Engineering, 111, José Pedro Drumond St., Belo Horizonte, Minas Gerais 30150-140, Brazil

Published online: 09 August 2023

time, in the USA, with the work of Osterberg [10]. According to the authors, this methodology would have the main advantage of separating the resistance portions of the shaft and the tip (or dummy tip, when the set of cells is far from the tip of the pile)—that is, there is no need for instrumentation and of a reaction system. The bidirectional test has been studied on several occasions, whether for comparison of the mechanical behavior with pile loaded from the top [1, 11, 12], interpretation of its results and conversion to a load-settlement curve equivalent to that obtained from the conventional load test [9, 11, 13–18] or, even, for just measurement of the ultimate bearing capacity of piles, mainly of large diameter drilled shafts. Despite the separation of the resistance plots without the use of instrumentation, the use of this technique allows a better understanding of the mechanical behavior of each segment and the soil–structure interaction in certain regions along the depth. Hence, the highlight of bidirectional test instrumentation in recent years in these types of piles, being used since then to evaluate the setup effect over time [19–21] to verify the bearing capacity of large diameter drilled shafts and their due design criteria [1, 3–5, 22], to study the influence that different excavation slurries could have on the mechanical behavior of these piles [4], to investigate possible adversities arising from the executive procedure of these types of piles [5], to investigate the influence that the post-injection phases in the shaft and/or in the tip would exert in large diameter drilled shafts [2, 8, 23–26] and to validate and/or compare with numerical models [12, 26–28].

Given this context, this paper presents the results of instrumented bidirectional static load tests carried out in two large diameter drilled shafts in sedimentary soil, typical of the coastal region of southern Brazil, which are part of the project for the VR Tower residential building, one of the tallest to be built in the country. Full-analyses are done through the instrumentation results and considerations are raised about the executive procedure of both piles, such as the loss of skin friction at the pile–soil interface, non-mobilization of the tip resistance and the possible existence of residual load along the shaft, a topic not yet addressed in the literature. The implementation of a simple algorithm is used to validate these results and, through the construction of the equivalent curve for both cases, to verify the design parameters according to the Brazilian standard.

2 Project Description

The VR Tower is the tallest building under construction built so far in the city of Itapema/SC, Brazil, being the first work of this size in the city. It is estimated that its height reaches the measure of 208 m referring to 51 floors in total, 50 of which are above ground level and one underground. It is one of the only national cases of buildings to exceed the 200 m height mark and makes Itapema the third Brazilian city to have a structure of this magnitude, category previously belonging only to the cities of Balneário Camboriú and São Paulo. When concluded, it will be the fifth tallest building in Brazil and the tallest among residential buildings with a single apartment per floor. Given the dimensions of the project, in-situ conditions, and constructive factors, large diameter drilled shafts proved to be the best option for the foundation of the building. In all, 54 piles with a diameter of 1.60 m and a length of 50 m will be uniformly distributed under the projection of the main tower, each with an estimated capacity around 10,000 kN, and another six piles with a diameter of 1.20 m and 40 m in length distributed over the remaining area, each with an estimated design load of 3500 kN. Figure 1 shows the distribution of the foundation elements, the test piles (P7 and P28) and the standard penetration test (SPT) and cone penetration test (CPT) carried out for the geotechnical characterization of the local subsoil.

3 Geological Conditions

The local geology of the city of Itapema is composed of three main systems. In stratigraphic order: basement dated from the Proterozoic to the Eo-Paleozoic period; recent continental-type sedimentary deposits, from the Pliocene to the Holocene (neogene to Quaternary); littoral, from the Pleistocene to the Holocene (Quaternary period) [29].

Six SPT and six CPT boreholes were drilled for subsoil investigation. Their distribution and distances to the tested piles are shown in Fig. 1: borehole SPT-05 is located 2.30 m from the center of pile P7 and holes SPT-01, SPT-02, and SPT-03 are located at a distance of P28 at 8.58 m, 6.18 m, and 11.25 m, respectively. Regarding the CPT, CPT-05 is located 1.50 m from P7 and the tests CPT-01 and CPT-06 are 8.66 m and 11.00 m away, in that order. The subsurface profile consists of the following eight types of soils and rocks: (1) embankment approximately 0.7 m at the surface; (2) 14.3 m layer of sand to silty sand, little to very compact, between 0.7 and 15 m; (3) 12 m of sandy to silty clay, very soft to soft, between 15 and 27 m; (4) 4 m of sand to clayey sand, medium to very compact, between 27 and 31 m; (5) 4 m of clay to silty clay, soft to hard density, between 31 and 35 m; (6) 3 m of sand to silty sand, with granulometry varying from fine to medium and density from medium to very compact, between 35 and 38 m; (7) 10 m of sandy clay to sandy silt, medium to very compact, between 38 and 48 m; and (8) segments with low quality rock and rock alterations (Rock Quality Designation less than 25%) below 48 m. For all SPT boreholes, the

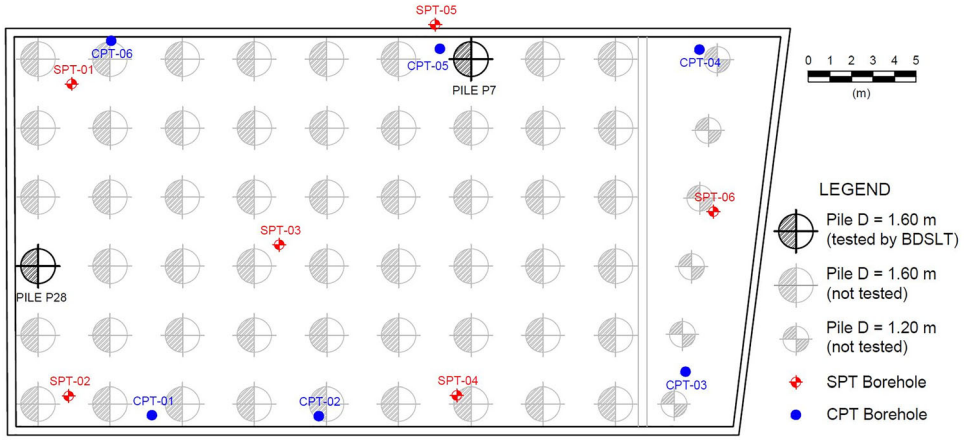

Fig. 1 Location of test piles and SPT and CPT tests

water table level was found to be around 1.4 m. The subsoil profile and the values found in the CPT and SPT tests are presented in Fig. 2, in which q_c is the cone tip resistance, f_s is the sleeve friction of the cone, F_r is the friction ratio (f_s/q_c) and $N_{SPT,60}$ is the number of samplers blows for a displacement of 30 cm, considering the energy of 60%.

4 Pile Installation, Test Setup and Field Test

The execution of the piles was done with rotary drilling with water circulation and clay-type stabilizing polymer MK AD until the rocky top was reached. This resulted in a final length of 48.4 m and 48.8 m for piles P7 and P28, respectively, and a diameter of 1.6 m for both. These lengths were excavated until rock fragments were obtained as excavation material, since the maximum torque of the drill rig was not indicated for rock excavation. Furthermore, it was expected that the design load would be supported by shaft resistance, given the great depth of the rocky top. Both piles were reinforced longitudinally with 21 bars of 25 mm in diameter and transversely with stirrups of 12.5 mm in diameter, spaced every 30 cm from the tip to a depth of 8 m, a level from which corresponds the handle and which will be demolished later for basement construction. The handle was reinforced by 4 bars of 20 mm in diameter and stirrups of 12.5 mm in diameter every 1.2 m. All steel cage was made with CA-50 steel bars.

The instrumentation of the piles was carried out by a set of CA-50 steel bars, usually called "sister bars" (25 mm in diameter and 1.0 m in length), whose surfaces received electrical extensometers—two installed diametrically opposite in the form of a full bridge of Wheatstone in each "sister bar". In the field, the bars were positioned in diametrically opposed pairs next to the reinforcement of the piles in certain positions so that, after the lowering and joining of the reinforcement sections, they reached the previously determined levels. For each pile, a total of 5 levels were instrumented by strain gages, 4 above and 1 below the cell set for the P7 pile and 3 above and 2 below

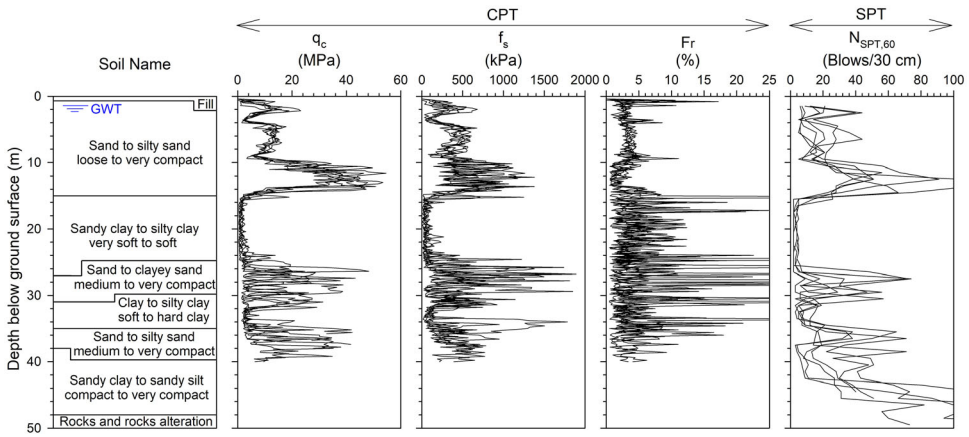

Fig. 2 Geotechnical profile and results of SPT and CPT tests

the cell set for the P28 pile. The instrumented bars were installed at a considerable distance from the load application point to avoid direct influences on them [30]. In addition, it was decided to install the last level of instrumentation 1 m above the tip to ensure that it would not be embedded in loose material, the existence of which was checked just before the piles were poured.

The set of expansive cells had three cells with 50 mm of linear course for both piles, totaling an area equal to 2886 cm^2 and 1356 cm^2 for piles P7 and P28, respectively. At the end of the installation, the set of expansive cells was at a distance of 5 and 10 m from the tip of piles P7 and P28, in that order, with depths of 43.4 and 38.8 m below the ground surface. Figure 3 shows the installation of the components of the bidirectional test in the reinforcement made in the field. After the descent of the reinforcements, concrete was pumped from bottom to top along the shaft to the depth of the handle of each pile (− 8 m). The concreting of the P7 pile was carried out the day after its excavation and the P28 pile was concreted immediately after its excavation. For the length of the handle, low-resistance mortar was used after the concrete had cured for subsequent cutoff. Figure 4 presents a scheme of soil distribution along the length of the piles after their completion, showing the location of the instrumentations and the set of expansive cells for each pile. To determine the soils in Fig. 4, borehole SPT-05 was used for pile P7, and the average between boreholes SPT-01 and SPT-02 for pile P28.

In Brazil, the bidirectional static load test is not standardized yet. Therefore, the tests were carried out on the piles per the Brazilian Standard for conventional static load testing [31]. The quick maintained load test (QMLT) was performed, which consists of the following processes: (1) the load must be applied in successive stages with values equal to or less than 10% of the estimated design load capacity and maintained for 10 min, regardless of the stabilization of settlements has been reached; (2) the displacement in each stage must be measured and recorded after 1 and 10 min after load application; (3) at the end of the last loading stage (twice the design load), the maximum load must be maintained for 2 h before the unloading phase begins and movement readings must be taken after 10, 30, 60, 90 and 120 min after load application; (4) the unloading must be carried out in at least four stages in relation to the maximum applied load, and displacement readings must also be taken after 1 and 10 min after the load is released; and (5) at the end of the last loading stage, the load must be maintained for 1 h and displacement measurements must be performed at times of 30 and 60 min. The loading stages carried out in this work were performed with load increments of 1150 kN and 600 kN for piles P7 and P28, respectively. Descending displacements from the top of the lower segment were monitored by three tell-tales positioned at the base of the set of expansive cells. For monitoring the top of the upper segment, a fixed bar attached to the tell-tale of the shaft, outside the pile, was used. Figure 5 presents a scheme of the main components used in the bidirectional test, where the distance between the supports of the reference beam to the center of the pile was 8 m.

5 Load Test Results and Analyses

5.1 Load–Displacement Responses

The load–displacement responses for both piles under bidirectional loading are shown in Fig. 6. Pile P7 was loaded to the 16th stage referring to a total load of 18,400 kN (9200 kN for each segment), at which stage the course of an of cells was exceeded and consequently the test had

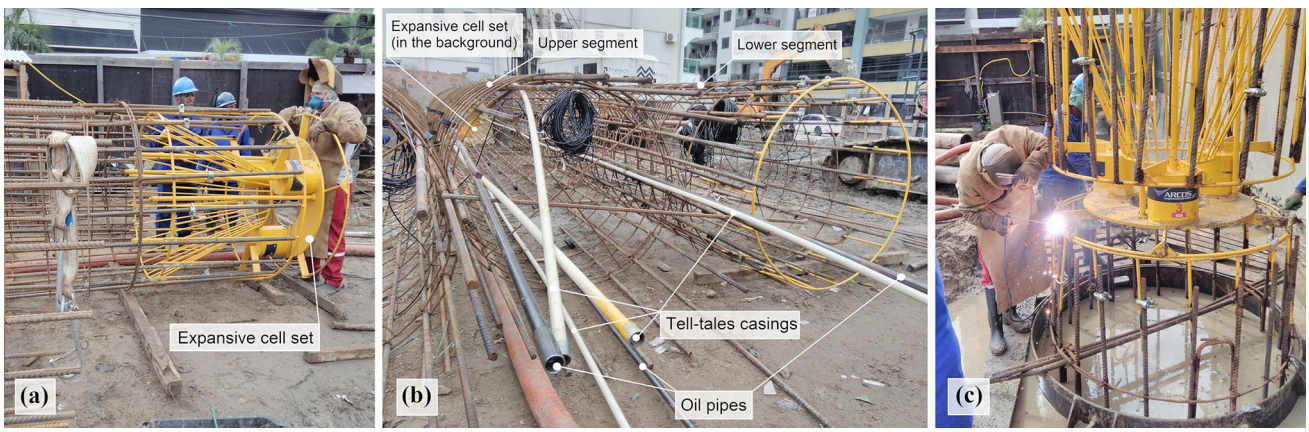

Fig. 3 Preparation of the bidirectional load test (**a**) installation of the set of expansive cells, **b** installation of the tell-tale casings, cell feed tubes and instrumentation, and (**c**) lowering of the steel cage

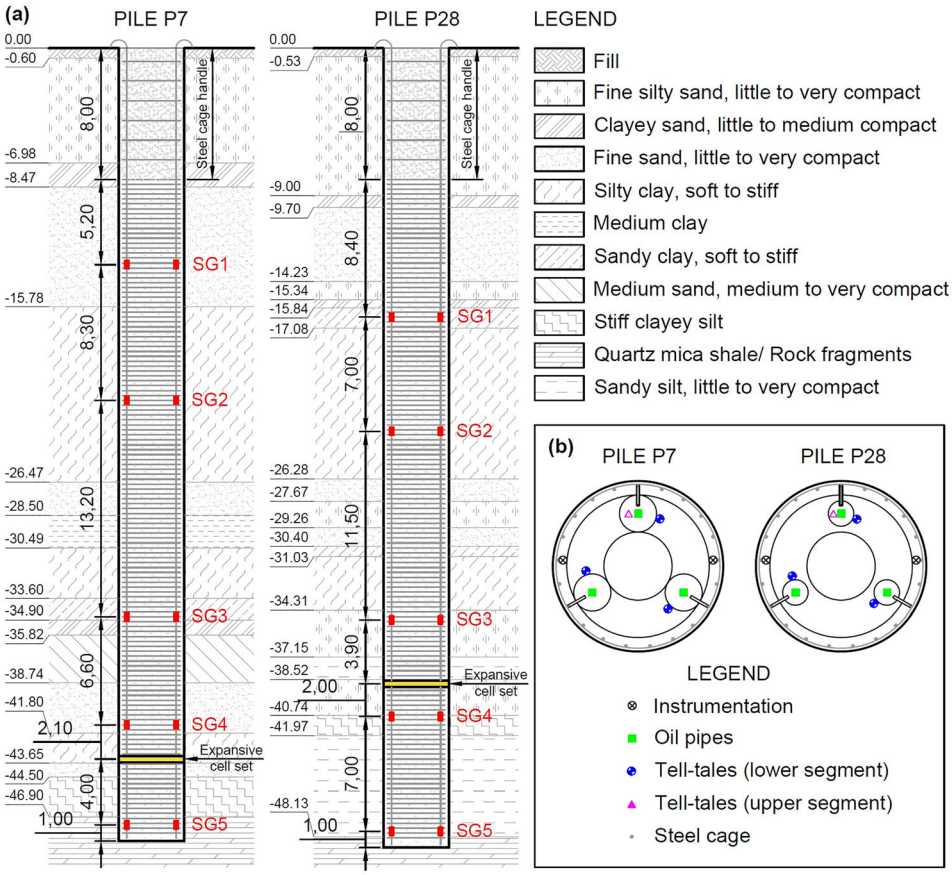

Fig. 4 Schematics of details of piles P7 and P28: **a** soil layering and instrumentation profiles, and **b** details of cross-sectional area for each pile

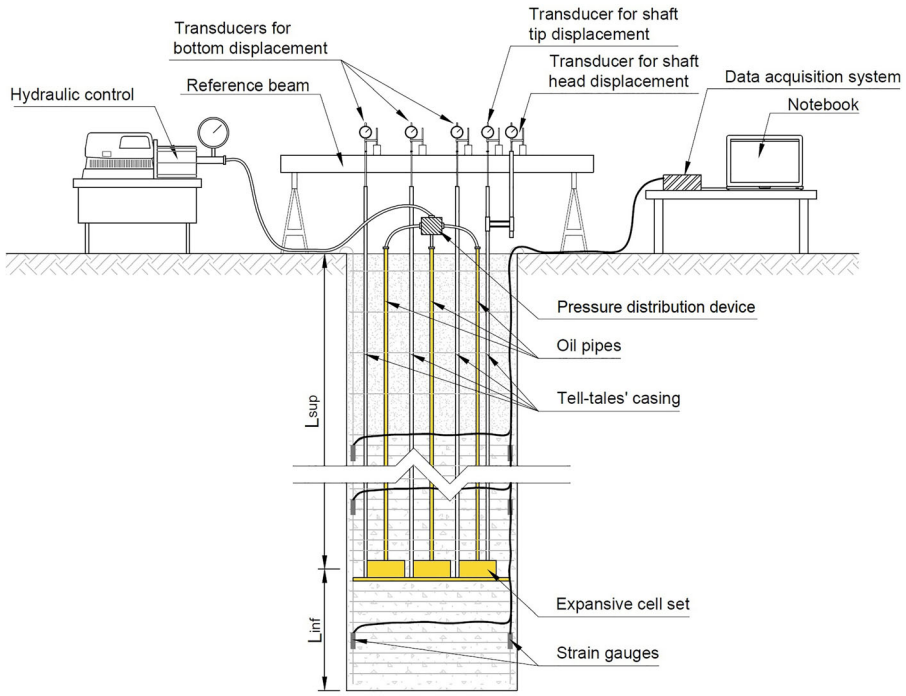

Fig. 5 Scheme for assembling the bidirectional test

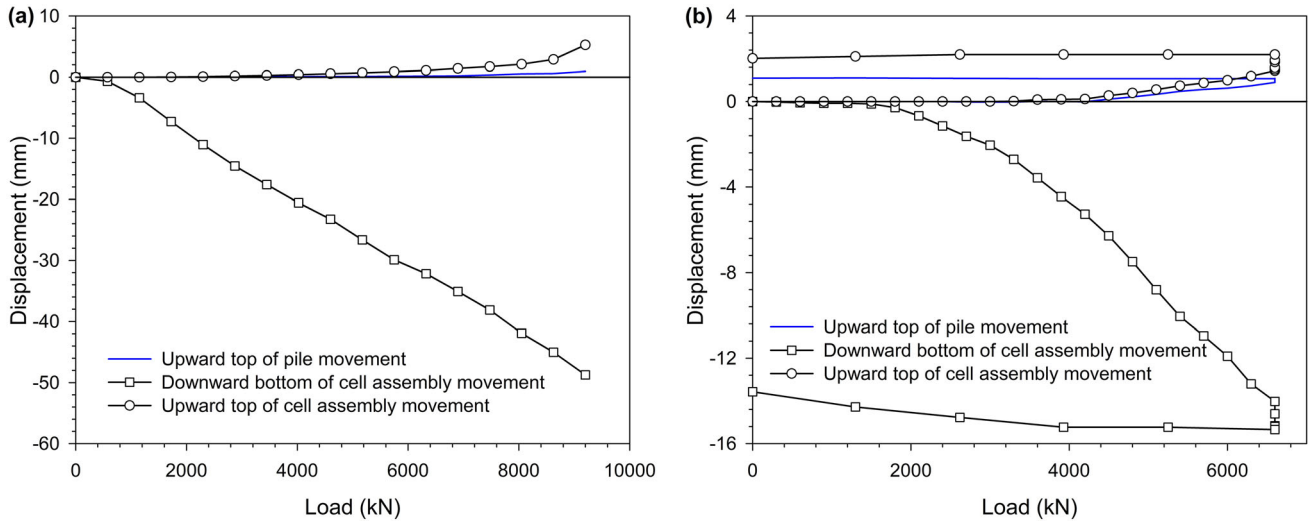

Fig. 6 Load–displacement responses for (**a**) pile P7 and **b** pile P28

to be interrupted. In this loading, the displacements of the upper and lower sections were equal to 5.25 and 48.73 mm, respectively. The unloading could not be performed due to the loss of the cell set. Pile P28 was loaded up to the 22nd stage for a total load of 13,200 kN (6600 kN for each segment), with displacements equal to 2.19 and 15.34 mm for the upper and lower segments, respectively. After unloading, the upper and lower sections showed residual displacements equal to 2.01 and 13.57 mm, in that order, and the test was declared concluded. It is noteworthy that the upper segment of pile P28 did not move up to a load of 3300 kN. Upward displacements are not imposed on the upper segment until the force applied by the expanding cell assembly exceeds the submerged weight of that segment plus any residual load developed along its length [1, 4, 30]. Considering the reinforced concrete specific weight of 25 kN/m^3, it is estimated that the submerged weight of the P28 pile shaft is 1200 kN, which would result in approximately 2100 kN in residual loads. This value, as will be demonstrated later in this work, does not represent reality. The displacement delay of the upper segment is possibly linked to the locking of the tell-tale positioned at the top of the set of expansive cells.

It is important to note from Fig. 6 that the shafts of both piles showed close displacement developments, although pile P7 was loaded at higher loads and, consequently, reached the transition range between the elastic and plastic regimes. As for the lower segment of the two piles, pile P28 showed less development of settlements for the same load, which can be explained by the greater length of its lower section and/or by better finishing conditions of its tip, since its concreting was carried out shortly after its excavation. The lower segment of the P7 pile presented an elastic regime, with no defined failure. A similar experience was evidenced in other works [3, 4, 6, 11, 17, 32] and can be explained from the following alternatives: (1) effect of the roughness of the shaft in the lower section, resulting in a relatively smooth surface with low adhesion between the pile and the soil and/or (2) presence of loose material at the tip [4]. The two possibilities will be discussed further later based on the instrumentation results.

5.2 Instrumentation Data and Load Transfer

Figure 7 presents the averages of responses of specific deformations as a function of the loads by the strain gauges in the five instrumented levels. For the P7 pile, the levels SG3 (34.7 m) and SG4 (41.3 m) presented close responses, with linear elastic behavior for strains above 8 με. This behavior was also observed for levels SG1 (13.2 m) and SG2 (21.5 m) throughout all loading stages. Furthermore, the loads that reached the SG5 level (47.4 m) were not supported by the tip (non-development of deformations in this region). This result can be explained by the accumulation of loose material at the tip of the pile due to its location very close to the set of expansive cells and/or concreting carried out 1 day after drilling the pile, even after checking the cleanliness its tip. For pile P28, close responses were found for levels SG3 (34.9 m) and SG4 (40.8 m), with the development of linear elastic behavior from 10 με. The levels SG1 (16.4 m) and SG2 (23.4 m) showed a decrease in the deformation gain for loads from 4800 kN; and a drop in the slope of the straight line was observed for the five levels from 6000 kN, indicating possible mobilization of lateral friction.

Unlike the conventional load test, the bidirectional test does not allow soil excavation around an instrumented

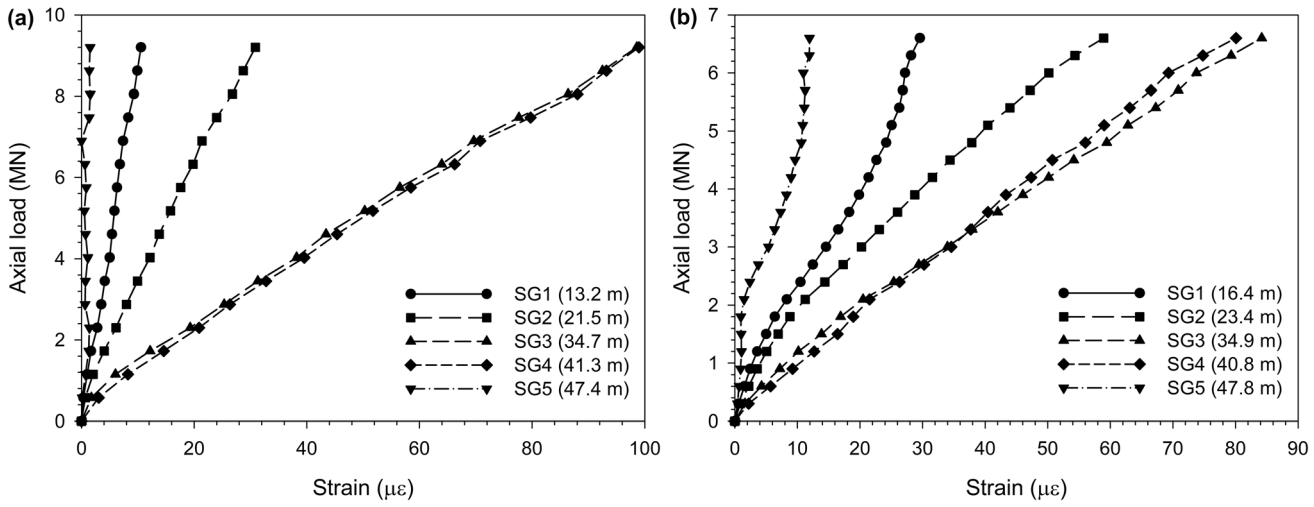

Fig. 7 Stress–strain responses of sister bars for (**a**) pile P7 and **b** pile P28

level for direct reading of the stress–strain behavior, called the reference section. Thus, the axial load transfer was obtained by the tangent/secant modulus method or the incremental stiffness method [30]. This method considers the inherent non-linearity and inelastic stress–strain response of concrete through the pile modulus as a function of imposed strain, which, after full mobilization of skin friction, is reduced with increasing stress or strain. Hence, the secant modulus of the pile is derived from the linear equation of the tangent modulus to determine the stress related to a given state of strain imposed on an instrumented section. When the shaft resistance above the gage location is fully mobilized, the tangent modulus exhibits decreasing linear behavior, which indicates the rate of decay of the pile's modulus of deformation. This magnitude is obtained by plotting the relationship between load increment and strain increment *vs* specific strain.

Figure 8 shows the tangent modulus *vs* deformation curves of both piles studied. Figure 8a shows that, for pile P7, the two sections of the upper segment closest to the load application point (SG3 and SG4 spaced at 8.7 m and 2.1 m, respectively) converged to a straight line even for small deformations, i.e., all the shaft resistance from the depth of 34.7 m to the depth of 43.4 m was fully mobilized in the first stages of loading, and this section represents the tangent modulus of a free column with the same properties as the pile without the effects of the adjacent soil. Linear regression of these results for tracing the line of the tangent module (Best fit line) provides the coefficients a and b of the equation. In this case, the average initial tangent modulus of the pile was 53.0 GPa, and the decay rate (slope of the tangent line) was − 0.222 GPa/με. As can still be seen from Fig. 8a, the SG2 level (21.5 m) was on the verge of linear behavior and tended toward the Best Fit Line, indicating that the section between SG3 and SG2 was close

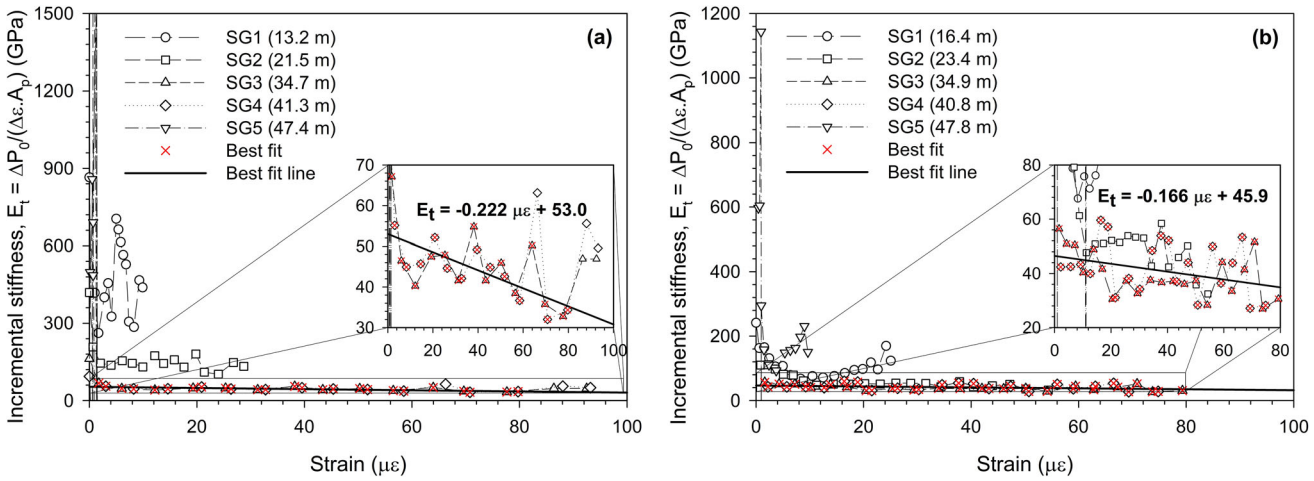

Fig. 8 Tangent moduli as a function of strains for (**a**) pile P7 and **b** pile P28

to mobilization. In addition, the high dispersion of the SG5 level (47.4 m) indicates that it is in loose material at the tip, preventing the mobilization of its resistance. Likewise, Fig. 8b shows that levels SG3 (34.9 m) and SG4 (40.8 m) located, respectively, 3.9 m above and 2.0 m below the set of expansive cells, converged to a straight line right in the first load stages, at low strains, demonstrating immediate mobilization of skin friction in these stretches. Level SG2 (23.4 m) also converged to this same line at strains around 12 με. In addition, levels SG1 (16.4 m) and SG5 (47.8 m) showed a tangent modulus gain as strains increased, indicating strain-hardening behavior. The average initial tangent modulus found was equal to 45.9 GPa and the decay rate was − 0.166 GPa/με. When compared to the deformation data of pile P7, readings at the tip level concerning pile P28 were already expected due to its greater distance from the set of expansive cells, ensuring better cleaning in this part, and concreting carried out right after its drilling.

The load distribution along the pile subject to the bidirectional loading test is shown in Fig. 9. Figure 9a shows that, for the lower segment of pile P7, all the load applied by the set of expansive cells was dissipated through skin friction due to the presence of loose material at the tip, which affects the development of its strength. For the upper segment, further analyses show instability in the slope of the curve between the load application point (43.4 m) and the SG4 level (41.3 m), indicating possible variations in skin friction in this region. Similar behavior is observed between levels SG4 (41.3 m) and SG3 (34.7 m) for loads greater than 2300 kN until reaching an almost vertical curve in the last loading stage. This performance can be explained by the existence of slurry filter cake between the pile and the surrounding soil, impairing its adherence and compromising the development of skin friction in these regions. This phenomenon was also observed in other cases of large diameter piles excavated with stabilizing fluid in sedimentary soils in the literature [4–6, 28] and confirmed by several laboratory tests [33–36]. Between levels SG3 (34.7 m) and SG2 (21.5 m), SG2 (21.5 m) and SG1 (13.2 m), and SG1 (13.2 m) and the ground surface there was a gradual development of the slope of the axial load transfer curve, with no evidence of side friction saturation or any possible anomaly.

Figure 9b shows that the tip strength (TR) of the lower segment of pile P28 started to develop at the stage referring to the 600 kN load. In the last loading stage, the tip of this portion had a capacity of 1077 kN, representing approximately 16% of the total load of 6600 kN applied in this segment. Furthermore, instabilities can be observed in the slope of the curve between the expansive cell set level (38.8 m) and the SG4 level (40.8 m). This phenomenon can be attributed to the existence of slurry filter cake between the pile and the soil, as mentioned earlier in the case of pile P7. The presence of this impermeable coating is also noted in the upper segment of pile P28, between the set of expansive cells and the SG3 level (34.9 m), being responsible for the decrease in the slope of this curve up to the load of 3300 kN, where the load at the level instrumented equals the applied load, that is, all shaft resistance is dissipated and the shaft acts as a free-length section. In

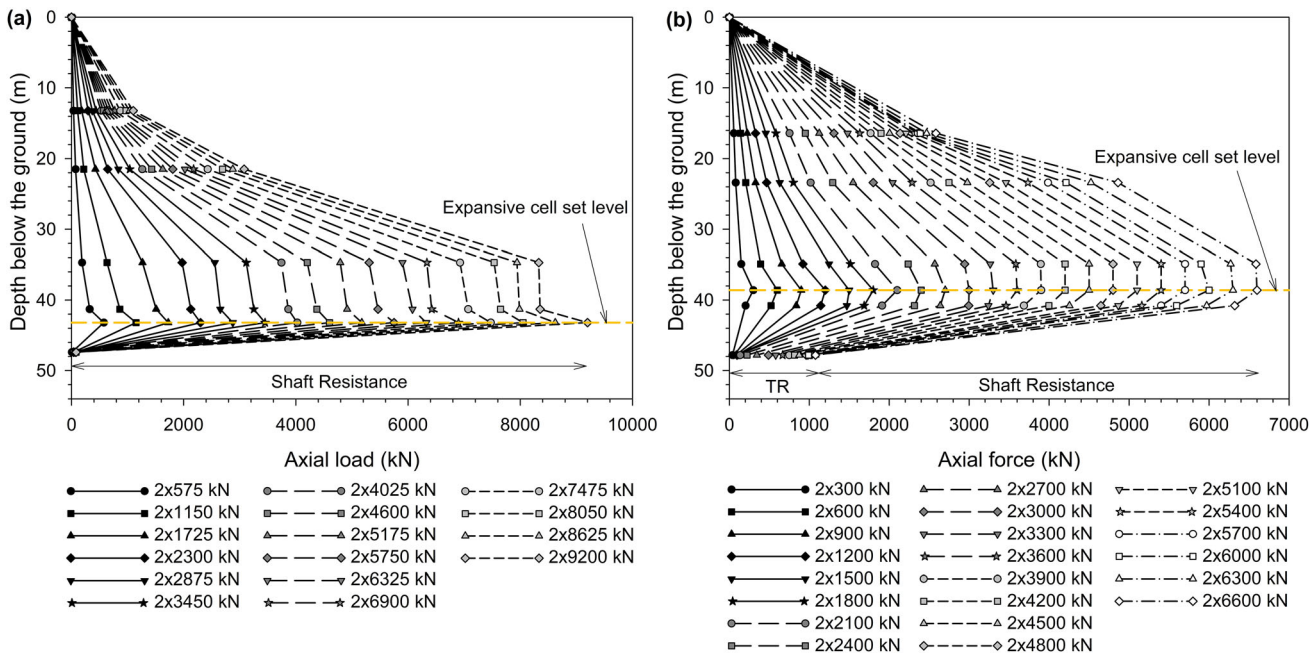

Fig. 9 Load distribution along the depth for (**a**) pile P7 and **b** pile P28

the sections from SG2 to SG3 (23.4 to 34.9 m) and from the ground surface to SG1 (0 to 16.4 m), further analyses show that the load transfer diagram had its shape modified up to the load of 5400 kN, indicating saturation skin friction in these segments and maintaining their inclination until the last loading stage. The load transfer diagram for the section located between levels SG2 (23.4 m) and SG1 (16.4 m) showed a gradual gain in inclination, indicating that skin friction was not fully mobilized along this section nor the occurrence of slurry filter cake in these regions.

As previously discussed, the pile section between the expansive cell group level (38.8 m) and the SG3 level (34.9 m) of pile P28 acted as the free-length section for applied loads above 3000 kN. In an analogy with the conventional static load test, SG3 acts as an instrumented level in a reference section, free of skin friction. In this way, the loads along the depth can be obtained directly by the secant modulus given by the following equation:

$$E_s = \frac{P_0}{A_p \varepsilon} \tag{1}$$

in which P_0 is the load applied by the hydraulic system and A_p is the pile section area. Figure 10a shows the secant modulus as a function of deformation for pile P28, highlighting the SG3 level and the best-fit line that describes its behavior. For comparison purposes, Fig. 10b presents the load distribution along the depth according to the secant and tangent moduli methods. As can be seen, all curves showed good similarity, regardless of the loading stage. The secant modulus method has as its main limitation the possible existence of residual loads on the shaft of the pile and the determination of its "absolute zero", while the tangent modulus method is not influenced by these same residual loads to determine the loads and stresses along the shaft [30]. Thus, the non-development of upward displacements in the upper segment of pile P28 for loads below 3300 kN, as previously discussed, is not due to the existence of residual loads in the pile, but to the malfunction of the tell-tale positioned for this reading.

5.3 Mobilized Shaft and Tip Resistances

Figure 11 illustrates the distribution of shaft resistance along the depth for piles P7 and P28. The skin friction of a generic layer i (τi) is calculated between two levels of consecutive strain gauges, as follows:

$$\tau_i = \frac{\Delta P_i}{\pi D L_i} \tag{2}$$

in which ΔP_i is the difference in load between two consecutive strain gauge levels, D is the pile diameter and L_i is the distance between two consecutive strain gage levels.

Figure 11a shows that, for most of the sections between strain gauges, the unit stress increased as the BDSLT loading stages. However, variations in the skin friction of the two segments just above the set of expansive cells were observed due to the presence of the slurry filter cake layer between the pile and the surrounding soil formed by the polymer, compromising the full development of the skin friction. Similar behavior before full mobilization was also observed in previous works [5, 23, 24]. Despite this, the segment just above this level (41.3 to 43.4 m) showed gradual skin friction gain after the 8050 kN load, totaling a value equal to 89 kPa in the last loading stage. On the other hand, the section situated between levels SG3 (34.7 m) and SG4 (41.3 m) showed loss of unit bond stress after a maximum value of 7.3 kPa referring to the load stage of 1725 kN, behavior of the post-peak softening type, reaching 0.7 kPa at the 9200 kN loading stage. Post-peak softening of unit stress for large diameter piles drilled with

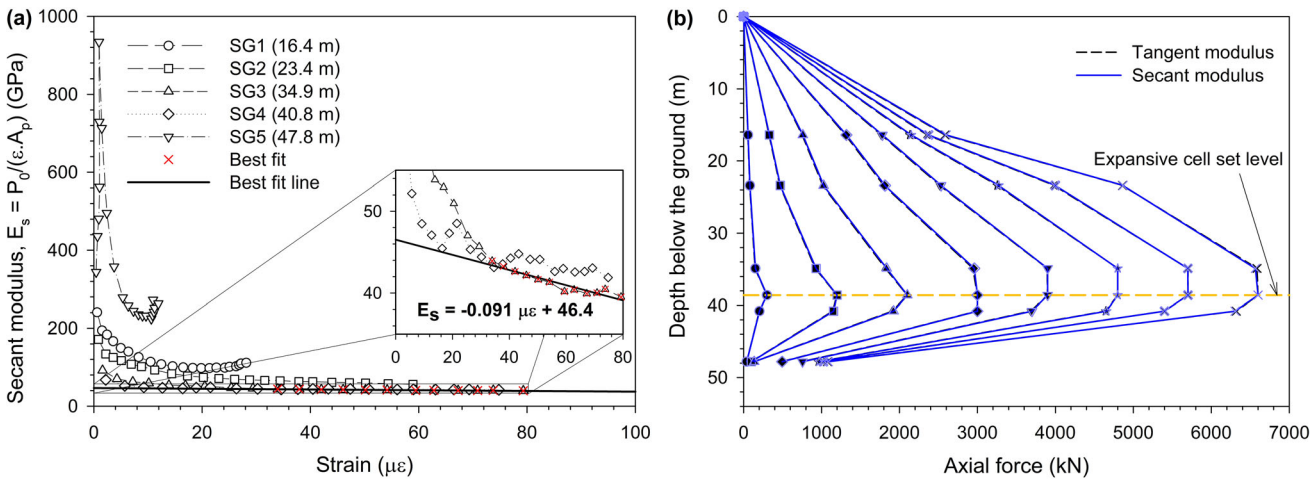

Fig. 10 **a** Secant modulus as a function of strain and **b** comparison between load distributions along the depth by the methods of secant and tangent moduli for pile P28

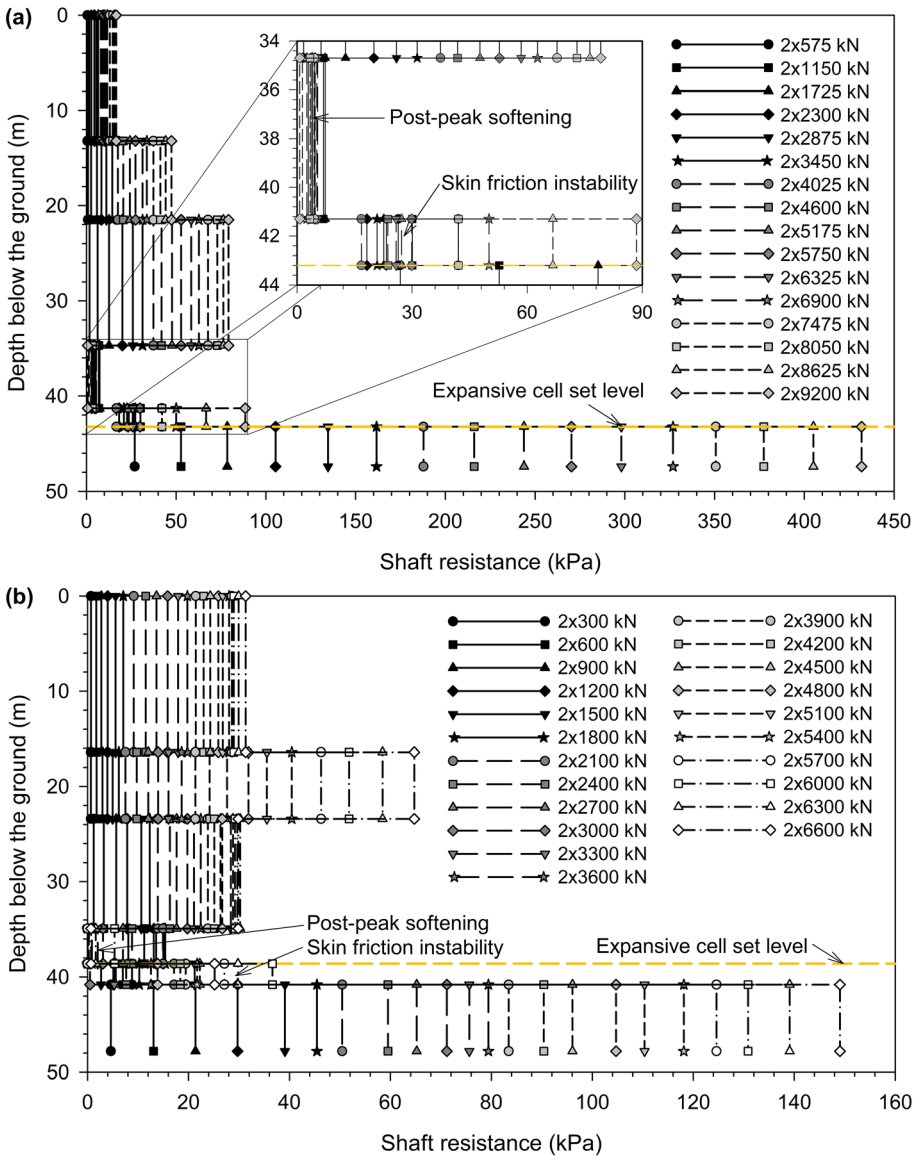

Fig. 11 Distribution of shaft resistance along the depth for **a** pile P7 and **b** pile P28

stabilizing fluid was also observed by other authors [4, 5, 7, 28]. The three other stretches of the upper segment between the ground surface and the SG3 level (34.7 m) showed skin friction stabilization in the later stages, i.e., all skin friction along this length was completely mobilized.

Post-peak softening behavior and instability in skin friction were also obtained for pile P28 in the segments between 34.9 m and 38.8 m (from SG3 to expansive cell set level) and 38.8 m and 40.8 m (from expansive cell set level to SG4), respectively, as can be seen in Fig. 11b. The post-peak softening behavior is also explained by the presence of slurry filter cake layer on the pile–soil interface, causing the pile to lose adherence to the soil when reaching a certain value of shaft resistance. Unlike the P7 pile, the instability of the unit shaft resistance of the P28 pile was maintained throughout the test. The behavior of the post-peak softening type, on the other hand, presented two peaks of skin friction: one equal to 15 kPa related to the load stage of 1200 kN and another of 5 kPa at the 6000 kN loading stage. Between loads of 3900 kN and 5700 kN and after the second peak, the skin friction of this segment was zero, that is, it behaved as a free-length section. The segments located between 0 m and 16.4 m (from the ground surface to SG1) and between 23.4 m and 34.9 m (from SG2 to SG3) both showed full mobilization of skin friction, reaching maximum value around 28 kPa in the stage referring to 5100 kN. In contrast, the segments located from SG1 (16.4 m) to SG2 (23.4 m) and from SG4 (40.8 m) to SG5 (47.8 m) did not show skin friction

stabilization, reaching shaft resistances of 65 kPa and 149 kPa in the last loading stage, respectively.

The complete shaft mobilization, skin friction instabilities, and post-peak softening behavior mentioned above are best visualized in the plot of mobilized shaft resistance *vs* relative pile–soil displacement shown in Figs. 12 and 13 for piles P7 and P28, respectively. The relative displacement of the shaft of a pile segment is estimated using Eqs. (3) and (4) as follows:

$$z_1 = z_0 - \frac{\Delta z_1}{2} \tag{3}$$

$$z_i = z_0 - \sum_{1}^{i-1} z_j - \frac{\Delta z_i}{2} \tag{4}$$

in which z_1 and z_i (i = 2, 3, 4, …) are the relative movements of the shaft of the first section and any section i, respectively, z_0 is the displacement at the load application point, and Δz_1 and Δz_i are the shortenings of the first section and any section i, in that order. It is noteworthy that Eqs. (3) and (4) apply to both the upper and lower segments and that, for the same load, both will not necessarily present the same displacement at the application point w_0. The shortening of any section i of the upper segment was calculated proportionally to its length L_i concerning the total shortening above the set of expansive cells [37], as shown in Eq. (5). The total shortening of the upper segment can be obtained directly from the bidirectional test by the difference between the upward displacement at the level of the expanding cell cluster and the displacement at the pile head. For the lower segment sections, the elastic shortening given by Eq. (6) was calculated as follows:

$$\Delta z_i = \frac{L_i}{L_{up}} \Delta z \tag{5}$$

$$\Delta z_i = \frac{P_{t,i} - P_{b,i}}{2E_p A_p} \Delta L_i \tag{6}$$

in which ΔL_i is the length of the segment i, i.e., the distance between two consecutive strain gauge levels, L_{up} is the total length of the upper segment of the pile, Δz is the total shortening of the upper segment of the pile, $P_{t,i}$ is the load at the top of a pile segment i, $P_{b,i}$ is the load at the base of a pile segment i, E_p is the modulus of elasticity of the pile (in the present work the average of the secant modulus given previously was used) and A_p is the area of the cross section of the pile.

Figure 12a shows the relation relative displacement of pile–soil vs shaft resistance for the upper segment of pile P7. As mentioned earlier, the first three stretches from the ground surface showed gradual development followed by full mobilization of skin friction up to 16.6, 47.4, and 79.2 kPa, respectively. The instability of the shaft resistance between the SG4 level (41.3 m) and the load application point (43.4 m) can be seen in Fig. 12a through the four peaks presented for frictions equal to 30.1, 23.3, 29.9 and 50.0 kPa at relative displacements of 0, 0.18, 0.85 and 50.04 mm, respectively, followed by hardening behavior in the last two loading stages. This instability is due to the presence of slurry filter cake in the pile–soil interface which, despite influencing the development of skin friction, did not restrain its mobilization in the last loading stages. Furthermore, there were no relative movements in this section until the fourth stage of loading. Post-peak softening behavior is also presented for the section between 34.7 and 41.3 m (SG3 to SG4), with peak friction equal to 5.1 kPa and residual friction of 0.7 kPa. Figure 12b presents the relationship relative displacement vs resistance of the shaft for the lower segment of pile P7, i.e., between the expansive cell array level and the SG5 level (47.4 m). As can be seen, the behavior of this section was elastic–linear,

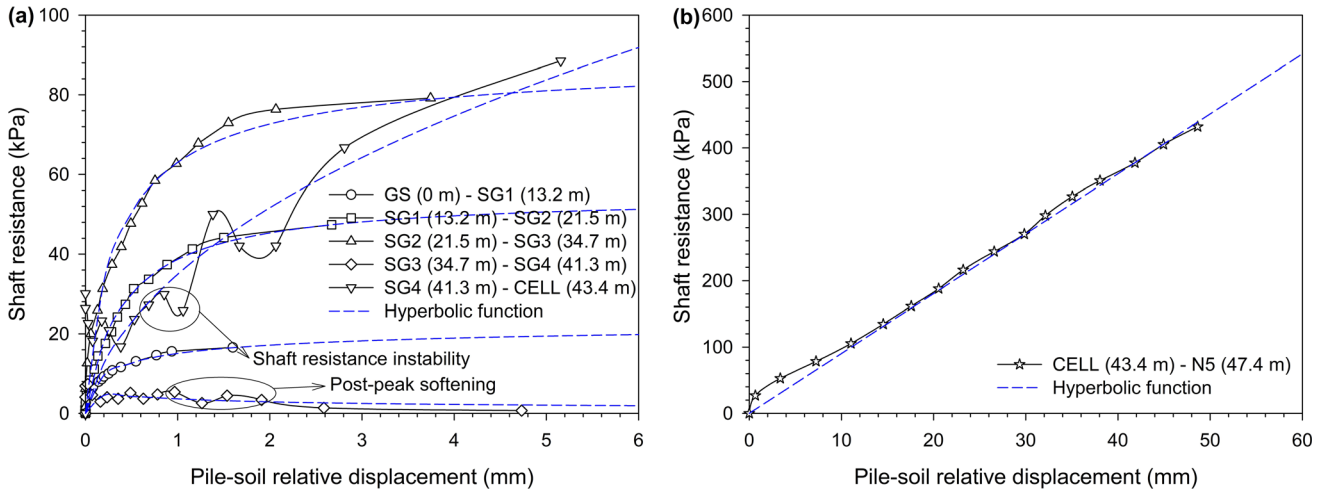

Fig. 12 Relationship between mobilized shaft resistance and relative pile–soil displacement for pile P7 in (**a**) upper and **b** lower segments

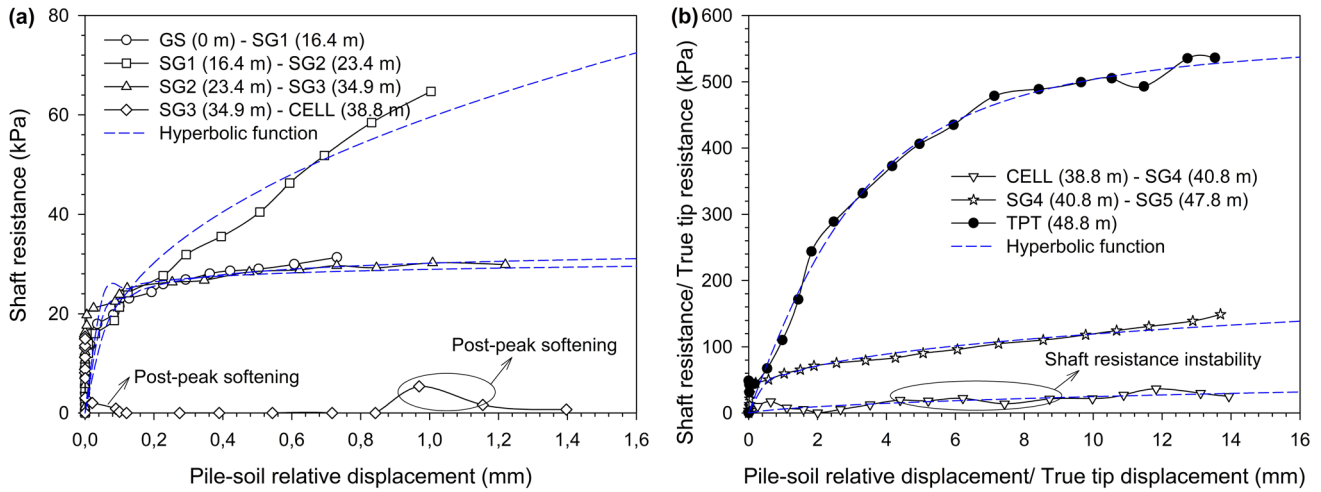

Fig. 13 Relationship between mobilized shaft resistance and relative pile–soil displacement and between true tip resistance and true tip displacement for pile P28 in (**a**) upper and **b** lower segments

mainly for friction above 100 kPa. The relationship relative displacement *vs* resistance of the lower segment tip (true pile tip) was not presented, because there was no development of tip resistance at any load stage.

Figure 13a shows the relationship relative pile–soil displacement *vs* shaft resistance for the upper segment of pile P28. The first and third stretches from the ground surface (0 to 16.4 m and 23.4 to 34.9 m, respectively) showed gradual development of skin friction until they were fully mobilized at 28 kPa with relative displacements around 0.36 and 0.48 mm, in that order. The second stretch (16.4 to 23.4 m) did not show shaft resistance mobilization, reaching 64.7 kPa referring to a relative displacement of 1 mm in the last loading stage. The section between the SG3 level (34.9 m) and the expansive cell set (38.8 m) did not develop skin friction except for two peaks equal to 15.4 and 5.4 kPa at relative movements of 0 and 0.97 mm, respectively. This post-peak softening type behavior was observed in the same region for pile P7, formed mainly by sand and silty sand of medium to high compactness. Figure 13b shows the relative pile–soil displacement *vs* shaft resistance of the lower segment of pile P28, as well as the displacement of its tip *vs* true tip resistance. Instability in skin friction between the expansive cell set level (38.8 m) and the SG4 level (40.8 m) was also observed, with peaks of 17.1, 19.4, 22.2 and 36.6 kPa referring to the relative displacements of 0.64, 4.40, 6.22 and 11.83 mm, respectively. The section between 40.8 and 47.8 m (SG4 to SG5) showed practically elastic–linear behavior for friction above 40 kPa. Unlike the P7 pile, the P28 pile showed the development of tip resistance without being fully mobilized, reaching a peak of 540 kPa with a displacement of 13.53 mm in the last load stage.

Several authors suggest that, while complete mobilization of skin friction is achieved for displacements of a few millimeters, the tip resistance is only fully mobilized for large displacements, on the order of 10–15% of its diameter [30, 38–41]. From Figs. 12b and 13b, it can be understood that the entire length below the set of expansive cells behaved as a pile tip for pile P7, especially because of its length. This idea is reinforced by the fact that its lower segment did not showed total mobilization, even for large relative displacements.

5.4 Algorithm for Load–Displacement Analysis of Bidirectional Static Load Tests

For a better understanding of the mechanisms involved, a load-transfer model was implemented for comparison with the results obtained in the field [42]. Due to the large variation in behavior, the load-transfer data were approximated to conventional hyperbolic functions [28], given by Eq. (7) and represented in Figs. 12 and 13 by the dashed lines:

$$f = \frac{k_m z}{\left[1 + \left(\frac{k_m z}{t_m}\right)^{hd}\right]^{1/d}} \tag{7}$$

in which f describes the mobilization of the shaft (τ) or tip (q_b) as a function of displacement z, k_m is the maximum soil stiffness (at z = 0), t_m is the coefficient related to maximum resistance, d the unitary resistance degradation parameter and h is the unit strength hardening parameter. The calibrated parameters for the load-transfer model are shown in Table 1 and were obtained by interpolation between the instrumentation data and the non-linear model given by the equation. The parameters for the true pile tip

Table 1 Calibrated parameters for load-transfer model

Pile	Segment	k_m (kPa/mm)	t_m (kPa)	d	h
P7	0 m–13.2 m	403	25	0.47	1
	13.2 m–21.5 m	136	55	0.98	1
	21.5 m–34.7 m	329	90	0.83	1
	34.7 m–41.3 m	61	8.3	1	1.38
	41.3 m–43.4 m	137	20	1	0.56
	43.4 m–47.4 m	9.02	–	–	0
P28	0 m–16.4 m	6610	35	0.49	1
	16.4 m–23.4 m	366	16	5	0.58
	23.4 m–34.9 m	6.2 10^6	35	0.25	1
	38.8 m–40.8 m	13	10	1	0.56
	40.8 m–48.8 m	309,428	1	1	0.68
	True pile tip	139	570	1.66	1

of pile P7 and between the depths of 34.9 m and 38.8 m of pile P28 are not presented, because they were considered zero in the simulation. In addition, the parameters determined for the segment between 43.4 m and 48.4 m of pile P7 describe the linear behavior presented during the test.

The load–displacement response of the pile submitted to the bidirectional test and performed in multilayer soils can be analyzed by sectioning each segment into n sections from the point of application of the load to its opposite extreme (pile tip for the lower segment and pile head for the upper segment). Figures 14a and 14b show the division scheme for the lower and upper segments, respectively. Thus, the load and the displacement at the load application point can be obtained from any base displacement z_b employing the flowchart shown in Fig. 15. The load–displacement curve is built from the algorithm processing for different base displacements. In Figs. 14 and 15, D is the pile diameter; E_p is the modulus of elasticity of the pile; A_p is the area of the pile section; Q_b is the load at the base of the analyzed segment (equal to zero for the upper segment); $q_b(z_b)$ is the unit base resistance of the analyzed segment, given by Eq. (7) for any displacement of the base z_b; $\tau_i(z_{m,i})$ is the lateral friction of any element i, given by Eq. (7) for any displacement in the middle of element $z_{m,i}$; $z_{b,i}$, $z_{m,i}$, $z_{t,i}$ are the displacements at the base, middle and top of any element i, respectively; $z'_{m,i}$ is the new displacement found in the middle of any element i; $P_{b,i}$ and $P_{t,i}$ are the loads at the base and at the top of any element i, respectively; ΔP_i is the difference between the loads at the top and at the bottom of any element i; Δz_i is the elastic shortening; and ΔL_i is the length of any element i. In this

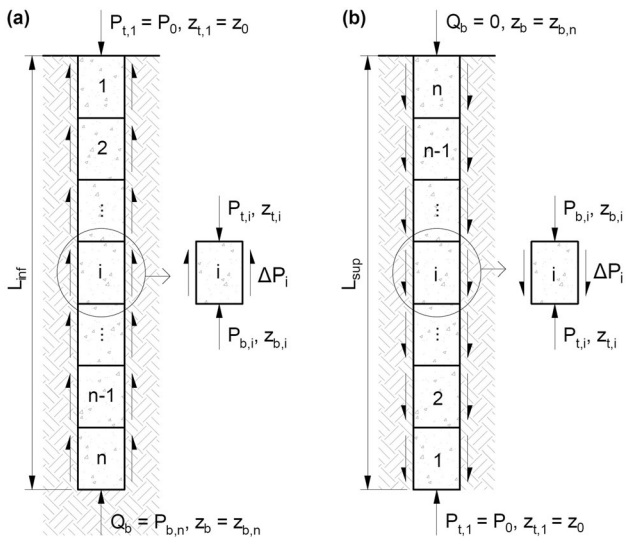

Fig. 14 Pile division scheme for load-transfer model for (**a**) lower and **b** upper segments

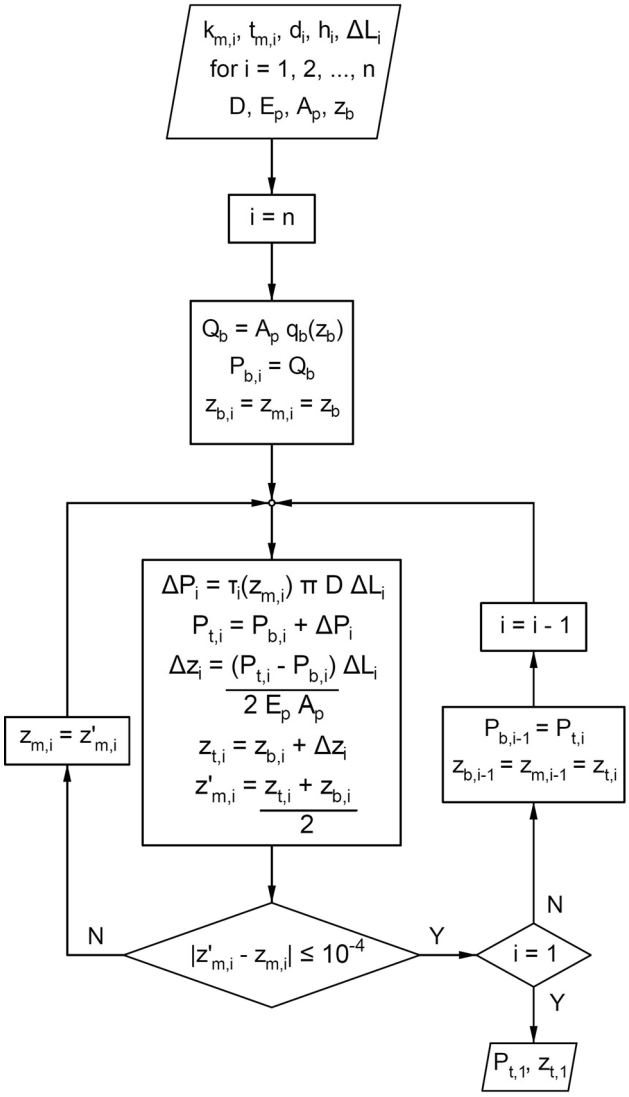

Fig. 15 Flowchart for implementing the algorithm

work, the modulus of elasticity was considered constant along the depth and equal to 53 and 45 GPa for piles P7 and P28, respectively.

Figure 16 shows the comparison between the results of the field test and the load-transfer model for the upper and lower segments of both tests. In general, the simulation showed good agreement with the field results, except the upper segment of pile P28. This discrepancy results from the tell–tale jamming for reading the upward movements of this pile. Despite this, shifting the field results at 1150 kN down, there is a good similarity with the load-transfer model in the last six loading stages. Furthermore, it can be seen from Fig. 16a that the lowest value of the simulated load–displacement curve is limited to a load of 4000 kN. This occurs, because the model starts from a displacement of the base of the shaft, i.e., it is assumed that lateral friction has been minimally mobilized along the entire shaft. To work around this situation, the simulation curve was extrapolated.

5.5 Equivalent Conversion Results

As the bidirectional test does not directly provide the ultimate load of the pile and the Brazilian standard does not provide a failure criterion for this test, it was decided to convert the results to those of a conventional test to evaluate the maximum load that the pile resists. For this, the traditional method of conversion [15, 16] was employed in which, for the same displacement, two loads are assigned, one for each segment, which are then added together. The elastic shortening related to the load applied to the upper segment was obtained through the test results (Fig. 6) and then added to the adopted initial displacement. This procedure was repeated for different adopted displacements, limited to the maximum displacement of the upper segment obtained in the test.

Figure 17 shows the equivalent curves which, for both cases, were far below the estimated ultimate load capacity (twice the design load of 11,500 and 6600 kN for piles P7 and P28, respectively) due to the low mobilization of the upper segment, resulting in a maximum test load of 9850 and 6150 kN for piles P7 and P28, in that order. To overcome this situation, the previously adopted load-transfer model was applied considering the load applied to the ground surface, that is, both segments moving from top to bottom simultaneously as a single pile. The same load-transfer functions and parameters used for the simulation of the bidirectional test were used [Eq. (7) and Table 1, respectively]. Adopting that the mechanical behavior of the pile–soil system is similar both in the upward and downward direction can provide minimally conservative results [12]. Furthermore, obtained considerable similarity in behavior between both displacements [11]. The simulation results are also shown in Fig. 17, showing good agreement with the equivalent curves within the displacement limit. The Brazilian standard NBR 6122 [43] defines the failure of the pile subjected to the conventional test as the load that intercepts the failure line given by Eq. (8). In this sense, the failure loads found for piles P7 and P28 were 23,000 and 26,600 kN, respectively, obeying a minimum load of twice the design load:

$$f = \frac{D}{30} + \frac{P_0 L}{A_p E_p} \tag{8}$$

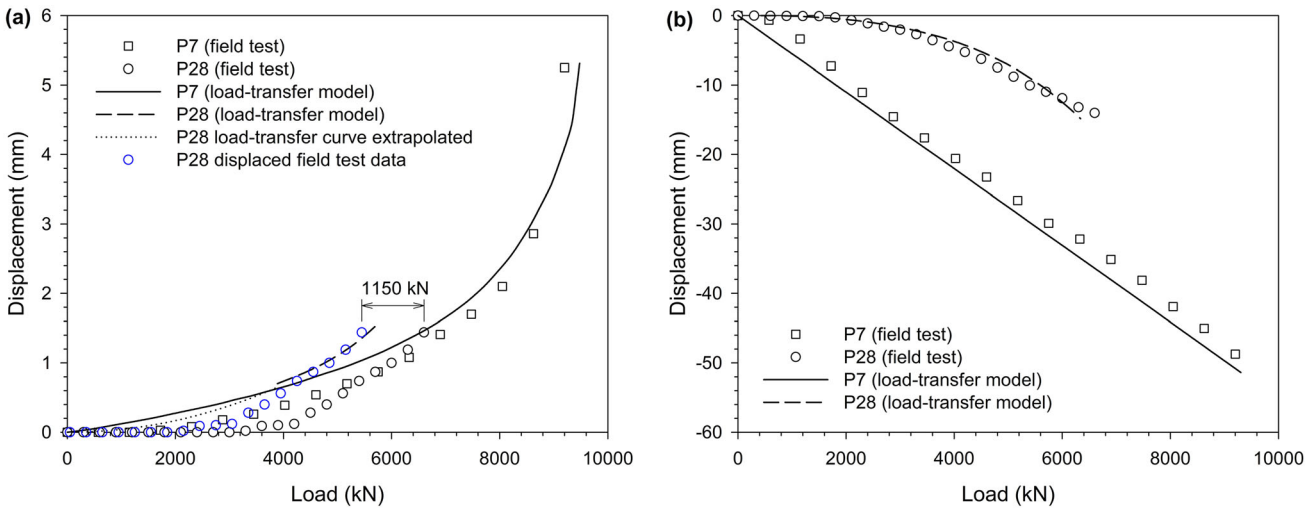

Fig. 16 Comparison between field test and load-transfer model results for (**a**) upper and **b** lower segments

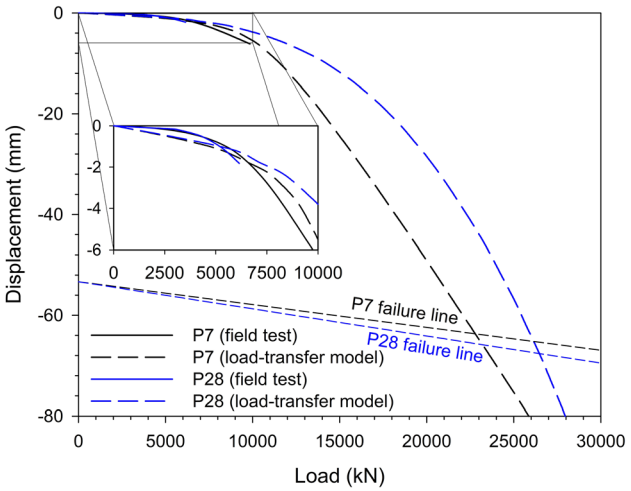

Fig. 17 Equivalent head-down curves and load-transfer model simulations

6 Summary and Conclusions

In this study, two large diameter drilled shafts with stabilizing polymer in highly heterogeneous sedimentary soil in the city of Itapema/SC, Brazil, were subjected to a bidirectional test to determine their ultimate load capacity. The same procedure was used for the execution of the two piles, with the difference between them restricted to the concreting of the P28 pile, carried out on the same day of its drilling, while in the P7 pile, the concreting was carried out on the following day. For analysis of the mechanical behavior, electrical extensometers were installed along the depth of the two piles. The load-transfer curves resulting from the instrumentation were approximated to hyperbolic functions and an algorithm based on the load-transfer model was implemented for the case of bidirectional load applied along the pile shaft. Curves equivalent to the conventional static load test were built using the field results and the processed algorithm—the results were used to determine the ultimate load capacities according to the Brazilian standard. Given the results and analyses carried out, it is concluded:

- The load-settlement curves of both piles showed the development of larger settlements in the segments below the set of expansive cells. For pile P7, the linear behavior of this section indicates the presence of loose material at its tip, which was later confirmed by the analysis of instrumentation results. When compared to the P28 pile, such behavior may be the result of the longer time between the end of drilling and the concreting of the excavation and/or the positioning of the set of expansive cells closer to the tip, which may have made it difficult to properly clean its tip;
- The results of the ascending load-settlement curve of pile P28 indicated the possibility of developing residual loads along its shaft. The portion between the load application point and the instrumented level just above acted as a free-length section due to the existence of a slurry filter cake, behaving as a reference section. The load distribution along the depth was calculated by secant modulus method [30], whose main limitation is the existence of residual loads, and was compared to the distribution obtained by the same author's tangent modulus method, which is not influenced by such loads. The similarity between the two results obtained rules out the possibility of the existence of residual loads on this pile; such responses of the load–displacement curve were attributed to the possible jamming of the tell-tale responsible for reading the ascending movements;
- Both piles showed instabilities in the development of lateral friction and post-peak softening behavior. This is a result of the deposition of slurry filter cake on the pile–soil interface, compromising the mobilization of lateral friction. Despite this, the lateral friction of most of the instrumented segments of the two piles reached complete mobilization;
- The hyperbolic model adopted to describe the load-transfer curves proved adequate. Its application in the implemented algorithm resulted in load-settlement curves in good agreement with the results of the bidirectional test, except for the case of the upward movements of pile P28, a correction for this curve being suggested.
- Due to the low displacements presented by the upper segments of both piles, it was not possible to determine the ultimate load capacities employing equivalent load-settlement curves constructed through field tests. The algorithm resulting from the hyperbolic model employed was used to construct the equivalent load-settlement curves for loads and displacements sufficient for determining the breaking load according to the Brazilian standard. The results succeeded to values higher than the estimated ones, even considering minimally conservative assumptions for the simulation.

Acknowledgements The authors gratefully acknowledge the support of the University of Campinas (Unicamp) and ARCOS Engineering and the National Council for the Improvement of Higher Education (CAPES) for the scholarships granted to the post-graduate students participating in the study.

Data availability Data supporting the findings of this study are fully available within the article.

Declarations

Conflict of Interest On behalf of all authors, the corresponding author states that there is no conflict of interest.

References

1. Fellenius BH, Ann TS (2010) Combination of O-cell test and conventional head-down test. Art of Foudation Engineering Practice. ASCE, West Palm Beach, Florida, USA, pp 240–259
2. Nguyen MH, Fellenius BH (2015) Bidirectional cell tests on non-grouted and grouted large-diameter bored piles. J Geo-Eng Sci 2(3–4):105–117. https://doi.org/10.3233/jgs-140025
3. Castelli RJ, Fan K (2002) O-Cell test results for drilled shafts in marl and limestone. Deep Foundations 2002: An International Perspective on Theory, Design, Construction, and Performance. ASCE, Orlando, Florida, USA, pp 807–823
4. Hai NM, Fellenius BH (2014) O-Cell tests on two 70-m long bored piles in Vietnam. From Soil Behavior Fundamentals to Innovations in Geotechnical Engineering: Honoring Roy E. Olson, ASCE, Atlanta, Georgia, USA, pp 482–496
5. Nguyen HM, Puppala AJ, Patil UD, Mosadegh L, Banerjee A (2017) Multi-level O-Cell tests on instrumented bored piles in the Mekong Delta. Geotechnical Frontiers 2017. ASCE, Orlando, Florida, USA, pp 274–283
6. Dao DH, Tran TQ, Congress SSC, Puppala AJ, Hai NM, Kim YS (2022) Evaluating the performance of large-diameter bored piles socketed in weathered rock. Indian Geotechnical J. https://doi.org/10.1007/s40098-022-00623-1
7. Lam C, Jefferis SA, Suckling TP, Troughton VM (2015) Effects of polymer and bentonite support fluids on the performance of bored piles. Soils Found 55(6):1487–1500. https://doi.org/10.1016/j.sandf.2015.10.013
8. Zhang Z, Gong W, Dai G, Cao X, Zhu Y, Huang H (2021) Field tests on bearing characteristics of large-diameter combined tip-and-side post grouted drilled shafts. Appl Sci 11(24):11883. https://doi.org/10.3390/app112411883
9. Silva PECAF (1983) Hydrodynamic Expansive Cells: A new way to perform load tests. Belo Horizonte (in Portuguese)
10. Osterberg JO (1989) New device for load testing driven piles and drilled shafts separates friction and end bearing. 14th International Conference of Piling and Deep Foundation. CRC Press, London, pp 421–427
11. Kwon OS, Choi Y, Kwon O (1936) Kim MM (2005) Comparison of the bidirectional load test with the top-down load test. Trans Res Record: J Trans Res Board 1:108–116. https://doi.org/10.1177/0361198105193600113
12. Russo G (2013) Experimental investigations and analysis on different pile load testing procedures. Acta Geotech 8(1):17–31. https://doi.org/10.1007/s11440-012-0177-4
13. Lee JS, Park YH (2008) Equivalent pile load-head settlement curve using a bi-directional pile load test. Comput Geotechnics 35(2):124–133. https://doi.org/10.1016/j.compgeo.2007.06.008
14. Kim HJ, Mission JLC (2011) Improved evaluation of equivalent top-down load-displacement curve from a bottom-up pile load test. J Geotech Geoenviron Eng 137(6):568–578. https://doi.org/10.1061/(asce)gt.1943-5606.0000454
15. Mission JLC, Kim HJ (2011) Design charts for elastic pile shortening in the equivalent top-down load-settlement curve from a bidirectional load test. Comput Geotech 38(2):167–177. https://doi.org/10.1016/j.compgeo.2010.11.001
16. Dai G, Gong W (2012) Application of bi-directional static loading test to deep foundations. J Rock Mechanics Geotech Eng 4(3):269–275. https://doi.org/10.3724/sp.j.1235.2012.00269
17. Kim SR, Chung SG (2012) Equivalent head-down load vs. movement relationships evaluated from bi directional pile load tests. KSCE J Civil Eng 16(7):1170–1177. https://doi.org/10.1007/s12205-012-1700-8
18. Massad F (2015) On the interpretation of the bidirectional static load test. Soils and Rocks 38(3):249–262
19. Kim SR, Chung SG, Fellenius BH (2011) Distribution of residual load and true shaft resistance for a driven instrumented test pile. Can Geotech J 48(4):583–598. https://doi.org/10.1139/t10-084
20. Abu-Farsakh MY, Haque MN, Tavera E, Zhang Z (2017) Evaluation of pile setup from osterberg cell load tests and its cost–benefit analysis. Transp Res Rec 2656(1):61–70. https://doi.org/10.3141/2656-07
21. Fellenius BH, Kim S-R, Chung S-G (2009) Long-term monitoring of strain in instrumented piles. J Geotech Geoenviron Eng 135(11):1583–1595. https://doi.org/10.1061/ASCEGT.1943-5606.0000124
22. Ann TS, Fellenius BH (2012) Failure of a barrette as revealed in an O-cell test. Full-Scale Testing and Foudation Design: Honoring Bengt H. Fellenius, ASCE, Oakland, USA, pp 307–321
23. Hu T, Dai G, Wan Z, Gong W (2022) Field study on the side resistance-softening and resistance-reinforcing effects of large-diameter combined grouting drilled shafts. Sustainability 14(11):6835. https://doi.org/10.3390/su14116835
24. Wan Z, Dai G, Gong W (2018) Full-scale load testing of two large-diameter drilled shafts in coral-reef limestone formations. Bull Eng Geol Env 77(3):1127–1143. https://doi.org/10.1007/s10064-017-1206-1
25. Wan Z, hui, Dai G liang, Gong W ming, (2019) Field study on post-grouting effects of cast-in-place bored piles in extra-thick fine sand layers. Acta Geotech 14(5):1357–1377. https://doi.org/10.1007/s11440-018-0741-7
26. Wan ZH, Dai GL, Gong WM (2020) Field and theoretical analysis of response of axially loaded grouted drilled shafts in extra-thick fine sand. Can Geotech J 57(3):391–407. https://doi.org/10.1139/cgj-2018-0382
27. Fellenius BH, Altaee A, Kulesza R, Hayes J (1999) O-Cell testing and FE analysis of 28 m deep barrette in Manila, Philippines. J Geotech Environ Eng 125:566–575
28. Pelecanos L, Soga K, Chunge MPM, Ouyang Y, Kwan V, Kechavarzi C, Nicholson D (2017) Distributed fibre-optic monitoring of an Osterberg-cell pile test in London. Géotechnique Letters 7:152–160. https://doi.org/10.1680/jgele.16.00081
29. Pires JDTS, Merege RCCB (2010) Project "Social-environmental diagnosis for creation of a conservation unit in Itapema/SC" - Final Report. Florianópolis, Brazil (in Portuguese)
30. Fellenius BH (2022) Basics of Foundation Design (Electronic Edition). https://www.felennius.net/papers/. Accessed 8 Aug 2022
31. ABNT (2006) NBR 12131: Pile static load test - test method. Brazil (in Portuguese), Rio de Janeiro
32. Castelli RJ, Wilkins E (2004) Osterberg load cell test results on base grouted bored piles in Bangladesh. GeoSupport 2004: Drilled shafts, Micropiling, deep mixing, remedial methods, and specialty foundation systems. ASCE, Orlando, USA, pp 587–602
33. Ata A, O'Neill M (2000) The physicochemical interaction between PHPA polymer slurry and cement mortar. Geotech Test J 23(2):225–235. https://doi.org/10.1520/GTJ11047J
34. Hu Z, McVay M, Bloomquist D, Herrera R, Lai P (2006) Influence of torque on lateral capacity of drilled shafts in sands. J Geotech Geoenviron Eng 132(4):456–464. https://doi.org/10.1061/(ASCE)1090-0241(2006)132:4(456)
35. Shakir RR, Zhu J (2010) An examination of the mechanical interaction of drilling slurries at the soil-concrete contact. J Zhejiang Univ, Sci, A 11(4):294–304. https://doi.org/10.1631/jzus.A0900456

36. Lam C, Jefferis SA, Martin CM (2014) Effects of polymer and bentonite support fluids on concrete–sand interface shear strength. Géotechnique 64(1):28–39. https://doi.org/10.1680/geot.13.P.012
37. Sinnreich J (2012) Strain gage analysis for nonlinear pile stiffness. Geotech Test J 35(2):367–374. https://doi.org/10.1520/GTJ103412
38. Hirayama H (1990) Load-settlement analysis for bored piles using hyperbolic transfer functions. Soils Found 30(1):55–64. https://doi.org/10.3208/sandf1972.30.55
39. Bersan S, Bergamo O, Palmieri L, Schenato L, Simonini P (2018) Distributed strain measurements in a CFA pile using high spatial resolution fibre optic sensors. Eng Struct 160:554–565. https://doi.org/10.1016/j.engstruct.2018.01.046
40. Zheng G, Peng SY, Ng CWW, Diao Y (2012) Excavation effects on pile behaviour and capacity. Can Geotech J 49(12):1347–1356. https://doi.org/10.1139/t2012-095
41. Zhang Q-Q, Zhang Z-M, Li S-C (2013) Investigation into skin friction of bored pile including influence of soil strength at pile base. Mar Georesour Geotechnol 31(1):1–16. https://doi.org/10.1080/1064119X.2011.626506
42. Coyle HM, Reese LC (1966) Load transfer for axially loaded piles in clay. J Soil Mechanics Foundations Division 92(2):1–26. https://doi.org/10.1061/JSFEAQ.0000850
43. ABNT (2019) NBR 6122: Design and execution of foudations. Brazil (in Portuguese), Rio de Janeiro